The influence of transformed Reynolds number suppression on gas transfer parameterizations and global DMS and CO_2 fluxes

Alexander Zavarsky[1] and Christa A. Marandino[2]

[1]Researcher, Kiel, Germany
[2]GEOMAR Helmholtz Centre for Ocean Research, Kiel, Germany

Correspondence: Alexander Zavarsky (alexz@mailbox.org)

Abstract. Eddy covariance measurements show gas transfer velocity suppression at medium to high wind speed. A wind-wave interaction described by the transformed Reynolds number is used to characterize environmental conditions favoring this suppression. We take the transformed Reynolds number parameterization to review the two most cited wind speed gas transfer velocity parameterizations, Nightingale 2000 and Wanninkhof 1992/2014. We propose an algorithm to correct for the effect of gas transfer suppression and validate it with two directly measured DMS gas transfer velocity data sets that experienced gas transfer suppression. A correction of the Nightingale 2000 parameterization leads to an average increase of 22 % of its predicted gas transfer velocity. The increase for Wanninkhof 2014 is 9.85 %. Additionally, we applied our gas transfer suppression algorithm to global air-sea flux climatologies of CO_2 and DMS.The global application of gas transfer suppression leads to a decrease of 6-7 % for the uptake CO_2 by the oceans and to decrease of 11 % of oceanic outgassing of DMS. We expect the magnitude of Reynolds suppression on any global air-sea gas exchange to be about 10 %.

1 Introduction

Gas flux F between the ocean and the atmosphere is commonly described as the product of the concentration difference ΔC between the liquid phase (seawater) and the gas phase (atmosphere) and the gas transfer velocity k. ΔC acts as the forcing potential difference and k as the conductance, which includes all processes promoting and suppressing gas transfer. c_{air} and c_{water} are the respective air-side and water-side concentrations. H is the dimensionless form of Henry's law constant.

$$F = k \cdot \Delta C = k \cdot \left(\frac{c_{water}}{H} - c_{air}\right) \tag{1}$$

ΔC is typically measured with established techniques, although the distance of the measurements from the interface introduce uncertainties in the flux calculation. Parameterizations of k are another source of uncertainty in calculating fluxes. The flux F can be directly measured, for example with the eddy covariance technique, together with ΔC in order to derive k and estimate a k parameterization (Eq. (2)).

$$k = \frac{F}{\Delta C} = \frac{F}{\frac{c_{water}}{H} - c_{air}} \tag{2}$$

It is very common that k is parameterized with wind speed and all wind speed parameterizations have in common that k increases monotonically with increasing wind speed. This assumption is sensible, as higher wind speed increases turbulence both on the air and the water side and hence the flux. Additional processes like bubble generation can additionally enhance gas transfer. The total gas transfer velocity k_{total}, which is measured by eddy covariance or other direct flux methods, is split up into the water side gas transfer velocity k_{water} and the air side gas transfer velocity k_{air} (Eq. (3)).

$$\frac{1}{k_{total}} = \frac{1}{k_{water}} + \frac{H}{k_{air}} \quad (3)$$

We focus, in this work, on k_{water} which is the sum of the interfacial gas transfer k_o and the bubble mediated gas transfer k_b (Eq. (4)).

$$k_{water} = k_o + k_b \quad (4)$$

To make gas transfer velocities of different gases comparable, Schmidt number (Sc) (Eq. (5)) scaling has been introduced. Sc scaling only applies to k_o and k_{air}. Sc is the ratio of the viscosity ν to the diffusivity D of the respective gas in seawater.

$$Sc = \frac{\nu}{D} \quad (5)$$

$$\frac{k_{o,Sc}}{k_{o,660}} = \left(\frac{Sc}{660}\right)^n \quad (6)$$

The exponent n is chosen depending on the surface properties. For smooth surfaces n=$-\frac{2}{3}$ and rough wavy surfaces n=$-\frac{1}{2}$ (Komori et al., 2011). In this study n=$-\frac{1}{2}$ is used.

In contrast to commonly accepted gas transfer velocity parameterizations, parameterizations based on direct flux measurements by eddy covariance systems have shown a decrease or flattening of k with increasing wind speed at medium to high wind speed (Bell et al., 2013, 2015; Yang et al., 2016; Blomquist et al., 2017).

We use the transformed Reynolds number Re_{tr} (Zavarsky et al., 2018) to identify instances of gas transfer suppression.

$$Re_{tr} = \frac{u_{tr} \cdot H_s}{\nu_{air}} \cdot cos(\theta) \quad (7)$$

Re_{tr} is the Reynolds number transformed into the reference system of the moving wave. u_{tr} is the wind speed transformed into the wave's reference system, H_s, the significant wave height, ν_{air} the kinematic viscosity of air and θ the angle between the wave direction and direction of u_{tr} in the wave's reference system. A flux measurement at values of $|Re_{tr}| \leq 6.96 \cdot 10^5$ is gas transfer suppressed (Zavarsky et al., 2018). It is a binary view, but in aerodynamics stall conditions, flow detachment and reattachment are binary as well, so we adopted this view. Describing transition conditions is beyond the scope of the first introduction of this model. This parameterization by Re_{tr} shows that the suppression is primarily dependent on wind speed, wave speed, wave height and a directional component. It is noteworthy that, so far, only eddy covariance deduced gas transfer velocities have shown a gas transfer suppression. This may be due to the spatial (1 km) and temporal (30 min) resolution of EC measurements, or to the types of gases measured (e.g. CO_2, DMS, OVOCs). The use of rather soluble gases (DMS, acetone, methanol) makes the gas transfer velocity not greatly influenced by bubble mediated gas transfer. Gas transfer suppression only affects k_o(Zavarsky et al., 2018). Another direct flux measurement technique, the dual tracer method, utilizes sulfur hexafluoride (SF_6) or ^{3}He. The dual tracer measurement usually lasts over few days but could have a similar spatial resolution as eddy covariance. SF_6 and ^{3}He are both very insoluble and heavily influenced by the bubble effect. Hence, if the gas transfer suppression only affects k_o, k_b could be the dominant process and masking the gas transfer suppression. Additionally, the long measurement period could decrease the likelihood of detection of gas transfer suppression as the conditions for suppression might not be persistent over a few days.

There are two main goals of this study: [1] develop and use a simplistic algorithm to correct for gas transfer suppression; [2] illustrate that gas transfer suppression is ubiquitous, showing up in our most used gas transfer parameterizations. To address goal 1, we develop a gas transfer suppression model and apply it to two DMS EC data sets. To address goal 2, we investigate the two most commonly used gas parameterizations (both cited more than 1000 times each) for the occurrence of gas transfer suppression. The Nightingale 2000 parameterization (N00) (Nightingale et al., 2000) contains data from the North Sea, Florida Strait and the Georges Bank between 1989-1996. The N00 parameterization is derived from changes in the ratio of SF^6 and ^{3}He (dual tracer method). We also investigate the Wanninkhof 2014 gas transfer parameterization (W14) (Wanninkhof, 2014) which is an update to Wanninkhof 1992 (Wanninkhof, 1992). Using a global ^{14}C inventory of the ocean they calculate the amount of CO_2 exchanged between the atmosphere and the ocean. This ^{14}C inventory is already influenced by gas transfer suppression, as it is globally averaged. They deduce a quadratic k vs wind speed parameterization using a wind speed climatology. Both k parameterizations (N00, W14) are monotonically increasing with wind speed.

In addition, we use wind wave data for the year 2014, calculate Re_{tr} and perform an analysis of the impact of gas transfer suppression on the yearly global air sea exchange of CO_2 and DMS. So far global estimates of air-sea exchange of these two gases(Lana et al., 2011; Takahashi et al., 2009; Rödenbeck et al., 2015) have been based on k parameterization which have not included a mechanism for gas transfer suppression. We provide an iterative calculation of the effect of gas transfer suppression and apply the correction to existing CO_2 and DMS climatologies.

2 Methods

2.1 Wave Watch Model III

We use wave data from the WWIII model hindcast run by the Marine Modeling and Analysis Branch of the Environmental Modelling Center of the National Center for Environmental Prediction (NCEP)(Tolman, 1997, 1999, 2009). The data was obtained for the total year 2014 with a temporal resolution of 3 hours and a spatial resolution of 0.5° x 0.5°. It also provides the u (meridional) and v (zonal) wind vectors, assimilated from the Global Forecast System, used in the model. We retrieved wind speed, wind direction, bathymetry, wave direction, wave period and significant wave height. We converted the wave period T_p to phase speed c_p, assuming deep water waves, using Eq. (8) (Hanley et al., 2010).

$$c_p = \frac{g \cdot T_p}{2\pi} \tag{8}$$

2.2 Auxiliary variables

Surface air temperature T, air pressure p, sea surface temperature SST and sea ice concentration were retrieved from the ERA-Interim reanalysis of the European Center for Meridional Weather Forecast(Dee et al., 2011). It provides a six hourly resolution and a global 0.125^o x 0.125^o spatial resolution. Sea surface salinity (SSS) was extracted from the Takahashi climatology (Takahashi et al., 2009).

Air-sea partial pressure difference (ΔpCO_2) was obtained from the Takahashi climatology. ΔpCO_2, in the Takahashi climatology, is calculated for the year 2000 CO_2 air concentrations. Assuming an increase in both the air concentration and the partial pressure in the water side, the partial pressure difference remains constant. The data set has a monthly temporal resolution, a 4^o latitudinal resolution and a 5^o longitudinal resolution.

DMS water concentrations were taken from the Lana DMS climatology (Lana et al., 2011). These are provided with a monthly resolution and a 1^o x 1^o spatial resolution. The air mixing ratio of DMS was set to zero $c_{air,DMS} = 0$. Taking air mixing ratios into account, the global air sea flux of DMS reduces by 17 %(Lennartz et al., 2015). We still think that our approach is reasonable, as we are looking at the change of flux due to gas transfer suppression only.

We linearly interpolated all data sets to the grid and times of the WWIII model.

2.3 Kinematic viscosity

The kinematic viscosity ν of air is dependent on air's density ρ and the dynamic viscosity μ of air, Eq. (9).

$$\nu(T,p) = \frac{\mu(T)}{\rho(T,p)} \tag{9}$$

The dynamic viscosity is dependent on temperature T and can be calculated using Sutherland's law(White, 1991) (Eq. (10)).

$$\mu = \mu_0 \cdot \left(\frac{T}{T_0}\right)^{\frac{2}{3}} \tag{10}$$

$\mu_0 = 1.716 \cdot 10^{-5}$ N s m^{-2} at $T_0 = 273$ K(White, 1991). Air density is dependent on temperature T and air pressure p and was calculated using the ideal gas law.

2.4 Transformed Reynolds number

The Reynolds number describes the balance of inertial forces and viscous forces. It is the ratio of the typical length and velocity scale over the kinematic viscosity. The transformed Reynolds number, in Eq. (11), uses the wind speed u_{tr}, transformed into the wave's reference system. The significant wave height H_s is used as the typical length scale. The difference between wind direction and wave direction is given by the angle θ. Between $\theta = 0^o$ and $\theta = 90^o$ the air flowing over the wave experiences, due to the angle of attack, a differently shaped and streamlined wave. The factor cos(θ) is multiplied to H_s to account for directional dependencies and shape influences (Fig. (A1)).

$$Re_{tr} = \frac{u_{tr} \cdot H_s}{\nu} \cdot cos(\theta) \tag{11}$$

3 Gas transfer suppression model

Below $|Re_{tr}| \leq 6.96 \cdot 10^5$ flow separation between the wind flowing above the wave and the flow entering the trough suppresses gas transfer (Zavarsky et al., 2018). As a result, common wind speed parameterizations of k are not applicable (Eq. (1)). To provide a magnitude of this suppression we propose an alternative wind speed u_{alt}, which is lower than u_{10}. This decrease accounts for the effect of gas transfer suppression. u_{alt} represents the wind speed with the maximum possible k in these conditions, hence an increase of u beyond u_{alt} does not result in an increase of k. u_{alt} can then be used with k parameterizations to calculate the gas flux.

Given a set wave field (constant H_s, wave direction and speed), if the relative wind speed in the reference system of the wave u_{tr} is big enough that $|Re_{tr}| > 6.96 \cdot 10^5$, no suppression occurs. In the 'no-suppression' case, k can be estimated by common gas transfer parameterizations. If the wind speed u_{10}, in the earth's reference system, is getting close to the wave's phase speed, u_{tr} in the wave's reference system gets smaller and $|Re_{tr}|$ drops below the threshold, flow separation happens, and suppression occurs. We propose a stepwise (Δs) reduction of u_{10} to calculate when the wind-wave system changes from the flow separation regime $\left(|Re_{tr}| < 6.96 \cdot 10^5\right)$ into a normal flow regime $\left(|Re_{tr}| > 6.96 \cdot 10^5\right)$. This can be used to estimate the magnitude of the suppression. We recalculate Re_{tr} with a lower $u_{alt} = u_{10} - i \cdot \Delta s$ and iterate i=0,1,2,3... as long as Re_{tr} is below the threshold (flow separation). If Re_{tr} crosses to the non-suppressing regime, the iteration is stopped and the actual u_{alt} can be used as an alternative wind speed. The iteration steps are: [1] Calculate Re_{tr}, using $u_{alt} = u_{10} - i \cdot \Delta s$.[2] Determine if $|Re_{tr}| \leq 6.96 \cdot 10^5$ [3] If yes, i=i+1 and continue with step [1]. If no, break the loop. The step size in this model was 0.3 m s^{-1}. We think this step size allows a good balance between computing time and velocity resolution. The minimum velocity for u_{alt} is 0 m s^{-1}. Figure 1 shows a flowchart of the algorithm. This algorithm is applied to every box at every time step.

A change in the parameters of the wave field is, in our opinion, not feasible as the wave field is influenced to a certain extent by swell which is externally prescribed. Swell travels long distances and does not necessarily have a direct relation to the wind conditions at the location of the gas transfer and measurement. Therefore, we change the wind speed only.

3.1 Gas transfer

The difference between u_{alt} and u_{10} directly relates to the magnitude of gas transfer suppression. u_{alt} can be used in two ways:[1] u_{10} can be directly replaced by u_{alt}. This is only possible for parameterizations with a negligible bubble contribution (like DMS), as we assume that the gas transfer suppression only affects k_o. As a result, one gets a k estimation using the lower wind speed u_{alt}. This is an estimate of the reduction of k by gas transfer suppression. [2] For parameterizations of rather insoluble gases, like CO_2, SF_6, ^3He, one needs to subtract Δk from the unsuppressed k parameterization. This correction is done by inserting $u_{10} - u_{alt}$ into a k_o parameterization (Eq. 12) and subtracting Δk. In this manuscript ZA18 from Zavarsky et al. (2018) is used as the parameterization of k_o. The magnitude of gas transfer suppression is given by Eq. 12.

$$\Delta k = k_o(u_{10}) - k_o(u_{alt}) = (3.1 \cdot u_{10} - 5.7) - (3.1 \cdot u_{alt} - 5.7) = 3.1 \cdot (u_{10} - u_{alt}) \tag{12}$$

For the global flux of DMS and CO_2 we use the bulk gas transfer formula (Eq. (1)). The global gas flux calculations are based on the following k parameterizations: ZA18 (for DMS), and the quadratic parameterizations, Tak09 (for CO_2) (Takahashi et al., 2009), W14 (for CO_2) and N00 (for DMS and CO_2). For every grid box and every time step we calculate u_{alt} according to the description in Sect. 3. If u_{alt} is lower than u_{10} from the global reanalysis then gas transfer suppression occurs. Subsequently, u_{alt} together with Eq. 12 is used in the specific bulk gas transfer formulas (Eq. (13-14)). For ZA18 u_{alt} can be directly inserted into this parameterization (Eq. (13)). However, all other parameterizations are based on measurements with rather insoluble gases, which have a significant bubble mediated gas transfer contribution. As a consequence we subtract the linear dependency Δk using the ZA18 parametrization, to account for the gas transfer suppression in k_o (Eq. (14)).

$$F_{lim,ZA18} = [k_{ZA18}(u_{10}) - \Delta k] \cdot \Delta C = (3.1 \cdot u_{alt} - 5.37) \cdot \Delta C \tag{13}$$

$$F_{lim,Tak00/W14/N00} = \left[k_{Tak00/W14/N00}(u_{10}) - \Delta k\right] \cdot \Delta C = \left[k_{Tak00/W14/N00}(u_{10}) - 3.1 \cdot (u_{10} - u_{alt})\right] \cdot \Delta C \tag{14}$$

For the global DMS transfer, we use the ZA18 and N00 parameterizations, as Lana et al. (2011) also uses N00.

Sea ice concentration from the ERA-Interim reanalysis was included as a linear factor in the calculation. A sea ice concentration of 90 %, for example, results in a 90 % reduction of the flux. Each time step (3 h) of the WWIII model provided a global grid of air-sea fluxes with and without gas transfer suppression. These single time steps were summed up to get a yearly flux result.

4 Results

We test the correction by shifting $u_{10} \rightarrow u_{alt}$ with two data sets of DMS gas transfer velocities, Knorr11 (Bell et al., 2017) and SO234-2/235 (Zavarsky et al., 2018). Both data sets experienced gas transfer suppression at high wind speed. Using this proof of concept, we quantify the influence of gas transfer suppression on N00 and W14 and correct for it. Finally, we apply the correction to global flux estimates of CO_2 and DMS.

4.1 Correction of the interfacial gas transfer

Fig. 2 and 3 show the corrected DMS gas transfer velocities for the SO234-2/235 and the Knorr11 cruises. We shift the measured data points, which are gas transfer suppressed, along the x-axis by replacing u_{10} with u_{alt}. The shift along the x-axis is equivalent to an addition of Δk to balance gas transfer suppression, see appendix. The black circles indicate the original data set at u_{10}. The colored circles are k values plotted at the corrected wind speed u_{alt}. If a black circle and a colored circle are concentric the data point was not suppressed and therefore no correction was applied. For comparison, the parameterization ZA18 is plotted in both figures. Both figures show the significant wave height with the color bar.

Fig. 2 illustrates the linear fits to the data set before (dotted) and after (dashed) the correction. The suppressed data points from 14-16 m s^{-1} moved closer to the linear fit after correction with u_{alt}. The large gas transfer velocity values at around 13 m s^{-1} and above 35 cm h^{-1} were moved to 11 m^{-1}. This means a worsening of the the k estimate by the linear fit. These data points have very low ΔC values (Zavarsky et al., 2018), therefore, we expect a large scatter as a result from Eq. (2).

Fig. 3 also shows an improvement of the linear fit estimates. The gas transfer suppressed data points were assigned the new wind speed u_{alt}, resulting in better agreement to ZA18. The change of the linear fit to the corrected and uncorrected data set can be seen in the dotted (before) and dashed (after) line. The corrected data points at 12-16 m s^{-1} are still, relative to the linear estimates, heavily gas transfer suppressed. A reason could be that the significant wave height of these points is larger than 3.5 m and they experienced high wind speed. A shielding of wind by the large wave or an influence of water droplets on the momentum transfer is suggested as reason (Yang et al., 2016; Bell et al., 2013). In principle, we agree that these processes may be occurring, but we hypothesize that it occurs only during exceptional cases of high winds and wave heights and that they are separately additionally on the gas transfer velocity. The Reynolds gas transfer suppression (Zavarsky et al., 2018) occurs over a larger range of wind speeds and wave heights, but obviously does not capture all the flux suppression. Therefore, it appears that several processes may be responsible for gas transfer suppression and they are not all considered in our model. This marks the upper boundary for environmental conditions for our model.

Tab. 1 shows the average offset between every data point and the linear fit ZA18. A reduction of the average offset can be seen for all data combinations. The last two columns of Tab. 1 show the mean absolute error. The absolute error also decreases with the application of our correction. The linear fits to the two data sets, before and after the corrections, are given in Tab. (2). The slopes for the two corrected data sets show a good agreement. However, we do not correct for the suppression entirely. The corrected slopes are both are in the range of the linear function ZA18 $k_{660} = 3.1 \pm 0.37 \cdot u_{10} - 5.37 \pm 2.35$ (Zavarsky et al., 2018), but the slopes barely overlap within the 95 % confidence interval.

4.2 Nightingale parameterization

The N00 parameterization is a quadratic wind speed dependent parameterization of k. It is widely used, especially for bulk CO_2 gas flux calculations as well as for DMS flux calculations in (Lana et al., 2011). The parameterization is based upon dual tracer measurements in the water performed in the North Sea (Watson et al., 1991; Nightingale et al., 2000) as well as data from the Florida Strait (FS) (Wanninkhof et al., 1997) and Georges Bank (GB) (Wanninkhof, 1992).

We analyzed each individual measurement that was used in the parameterization to asses the amount of gas transfer suppressing instances that are within the N00 parameterization. The single measurements, which are used for fitting the quadratic function of the N00 parametrization, are shown together with N00 in the left panel of Fig. 4. As the measurement time of the dual tracer technique is on the order of days, we interpolated the wind and wave data to 1 h time steps and calculated the number of gas transfer suppressing and gas transfer non-suppressing instances. The right panel of Fig. 4 shows the suppression index which is the ratio of gas suppressing instances to the number of data points (x-axis). The value 1 indicates that all of the interpolated one hour steps were gas transfer suppressed. The y-axis of Fig. 4 depicts the relation of the individual measurement to the N00 parameterization. A ratio (y-axis) of 1 indicates that the measurement point is exactly the same as the N00 parameterization. A value of 1.1 would indicate that the value was 10 % higher than predicted by the N00 parameterization.

We expect a negative correlation between the suppression index and the relation of the individual measurement vs the N00 parameterization. The higher the suppression index, the higher the gas transfer suppression and the lower the gas transfer velocity k with respect to the average parameterization. The correlation (Spearman's rank) is -0.43 with a significance level (p-value) of 0.11. This is not significant. However, we have to take a closer look at two specific points: [1] Point 11, GB11 that shows low measurement percentage despite a low suppression index, and [2] point 14, FS14 that shows high measurement percentage despite a high suppression index. GB11 at the Georges Bank showed an average significant wave height of 3.5 m, with a maximum of 6 m and wind speed between 9-13 m s^{-1}. Transformed wind speeds u_{tr} are between 4-20 m s^{-1}. As already discussed in Sect. 4.1 using the Knorr11 data set, wave heights above 3.5 m could lead to gas transfer suppression without being captured by Reynolds gas transfer suppression model (Zavarsky et al., 2018). High waves together with the strong winds could mark an upper limit of the gas transfer suppression model (Zavarsky et al., 2018). On the other hand the FS14 data point showed an average wave height of 0.6 m and wind speed of 4.7 m s^{-1}. It is questionable if a flow separation and a substantial wind wave interaction can be established at this small wave height. This could mark the lower boundary for the Reynolds gas transfer suppression model(Zavarsky et al., 2018). Taking out either or both of these measurements (GB11 or FS14) changes the correlation (Spearman's rank) to -0.62 p=0.0233 (no GB11), -0.59 p=0.033 (no FS14) and -0.79 p=0.0025 (no GB11, no FS14). All three are significant. The black solid line in the right panel of Fig. 4 is a fit, which is based on the Eq. (15), to all points but GB11 and FS14.

$$y(x) = a_1 + a_2 \cdot \frac{1}{x - a_3} \tag{15}$$

We choose this functional form, because we follow the finding that the effect of gas transfer suppression is not linear but rather has a threshold (Zavarsky et al., 2018). This means that the influence of suppression on gas transfer is relatively low with a small suppression ratio, but increases strongly. The fit coefficients are:a_1 =1.52, a_2=0.14 and a_3=1.18 .

Fig. 5 shows the, according to the gas transfer suppression model (Section 3), corrected data points. We do not correct the individual data points along the wind speed axis (x-axis), as the parameterization has a significant bubble contribution, but add Δk (Eq. 12) to make up for the suppressed part of total k.

A new quadratic fit was applied to the corrected data points ((Eq. 16), Fig. 5).

$$k_{660} = 0.359 \cdot u^2 \tag{16}$$

On average the new parameterization is 22 % higher than the original N00 parameterization. This increase is caused by the heavy gas transfer suppression of the individual measurements. As we believe that this suppression only affects the interfacial k_o gas exchange, it might not be easily visible (decreasing k vs u relationship) in parameterizations based on dual tracer gas transfer measurements because of the potential of a large bubble influence.

The calculation of the unsuppressed N00 parameterization is an example application for this correction algorithm. We do not advise using the unsuppressed N00 parameterization for flux calculations. We hypothesize that the N00 contains a large bubble component, as it is based on ^3He and SF_6 measurements, which compensates the gas transfer suppression. Therefore, N00 is suitable for CO_2 flux calculations.

4.3 Wanninkhof parameterization

The W14 parameterization estimates the gas transfer velocity using the natural disequilibrium between ocean and atmosphere of ^{14}C and the bomb ^{14}C inventories. The total global gas transfer over several years is estimated by the influx of the ^{14}C in the ocean(Naegler, 2009) and the global wind speed distribution over several years. The parameterization from W14 is for winds averaged over several hours. The WWIII model winds, used here, are 3 hourly and therefore in the proposed range(Wanninkhof, 2014). The W14 parameterization is given in Eq. (17).

$$k_{660,W14} = 0.251 \cdot (u_{10})^2 \tag{17}$$

The interesting point about this parameterization is that it already includes a global average gas transfer suppressing factor. The parametrization is independent of local gas transfer suppression events. It utilizes a global, annual averaged, gas transfer velocity of ^{14}C and relates it to remotely sensed wind speed. This means that the average gas transfer velocity has experienced the average global occurrence of gas transfer suppression and therefore is incorporated in the k vs u parameterization.

The quadratic coefficient a is calculated by dividing the averaged gas transfer velocity k_{glob} by u^2 and the wind distribution distu of u.

$$a = \frac{k_{glob}}{\sum u^2 \cdot distu} \tag{18}$$

The quadratic coefficient then defines the wind speed dependent gas transfer velocity k (Eq. (19)).

$$k = a \cdot u^2 \tag{19}$$

The left panel of Fig. 6 shows the global wind speed distribution of the year 2014 taken from the WWIII model, which is based on the NCEP reanalysis. Additionally, we added the distribution taking our wind speed correction into account. At the occurrence of gas transfer suppression we calculated, as described in Sect. 3, u_{alt} as the representative wind speed for the unsuppressed transfer. The distribution of u_{alt} shifts higher wind speed (10-17 m s^{-1}) to lower wind speed regimes (0-7 m s^{-1}). This alters the coefficient for the quadratic wind speed parametrization. A global average gas transfer velocity of k_{glob}=16.5 cm h^{-1}(Naegler, 2009) results in a coefficient a=0.2269, using the uncorrected NCEP wind speed distribution. With the u_{alt} distribution a becomes 0.2439. This is an 9.85 % increase. Our uncorrected value of a=0.2269 differs from the W14 value of a=0.251 because we use a different wind speed distribution. The W14 uses a Rayleigh distribution with $\sigma = 5.83$, our NCEP derived $\sigma = 6.04$ and the corrected NCEP $\sigma = 5.78$. This means that the W14 uses a wind speed distribution with a lower global average speed. However, for correction we use the relative gas transfer reduction between our calculated parameterization and our calculated and corrected parameterization. For the calculation of a, we did not use a fitted Rayleigh function but the corrected wind speed distribution from Fig. 6.

A comparison of W14, N00 and the corrected parameterizations is shown in the right panel of Fig. 6. N00 shows the lowest relationship between u and k. W14 shows a parameterization with a global averaged gas transfer suppression influence and is therefore slightly higher than N00. It appears that the gas transfer suppression is overcompensating the smaller bubble mediated gas transfer of CO_2 (W14). The corrected N00 is significantly higher than the W14+9.85 %. We hypothesize that this difference is based on the different bubble mediated gas transfer of He, SF_6, and CO_2.

4.4 Global Analysis

We used the native global grid (0.5^o x 0.5^o) from the WWIII for the global analysis. The data points from the DMS and CO_2 climatologies as well as all auxiliary variables were interpolated to this grid.

Fig. 7 shows the percentage of gas transfer suppressed data points with respect to the total data points for every month in the year 2014. The average yearly global percentage is 18.6 %. The minimum is 15 % in March and April and the maximum is 22 % in June, July and August. Coastal areas and marginal seas seem to be more influenced than open oceans. The reason could be that gas transfer suppression is likely to occur at developed wind seas when the wind speed is in the same direction and magnitude as the wave's phase speed. At coastal areas and marginal seas, the sea state is less influenced by swell and waves that were generated at a remote location. Landmasses block swell from the open ocean to marginal seas. The intra-annual variability of gas transfer suppression is shown in Fig. 8. Additionally, we plotted the occurrences split into ocean basins and Northern and Southern Hemisphere. Two trends are visible. There is a higher percentage of gas transfer suppression in the Northern Hemisphere and, on the time axis, the peak is in the respective (boreal and austral) summer season. The Southern Hemisphere has a water-landmass ratio of 81 %, the northern Hemisphere's ratio is 61 %. The area of free open water is therefore greater in the southern part. Fully developed seas without remote swell influence favor gas transfer suppression. In the Southern Hemisphere, the large open ocean areas, where swell can travel longer distances, provide an environment without gas transfer suppression. The peak in summer and minimum in winter can be associated with the respective sea ice extent on the Northern and Southern Hemisphere. Fig. 7 shows that seas, which are usually ice covered in winter, show a high ratio of gas transfer suppression.

The global reduction of the CO_2 and DMS flux is calculated using Eq. (13)-(14) and shown for every month in Fig. 9 and 10. Most areas with a reduced influx of CO_2 into the ocean are in the northern Hemisphere. The only reduced CO_2 influx areas of the Southern Hemisphere are in the south Atlantic and west of Australia and New Zealand. Significantly reduced CO_2 efflux areas are found in the northern tropical Atlantic, especially in the boreal summer months, the northern Indian Ocean and the Southern Ocean.

For the DMS flux (Fig. 9) the absolute values of reduction, due to gas transfer suppression, coincide with the summer maximum of DMS concentration and therefore large air-sea fluxes (Lana et al., 2011; Simó and Pedrós-Alió, 1999). In the boreal winter the northern Indian Ocean also shows a high level (10 μmol m^2 d^{-1}) of reduction. The highest water concentrations and fluxes in the Indian Ocean are found in boreal summer (Lana et al., 2011), which does not seem to be greatly influenced by gas transfer suppression.

The total amount of carbon taken up by the ocean is shown in Tab. 3. We calculate a total carbon uptake for the year 2014 of 1.15 Pg C for the N00 parameterization without the effect of gas transfer suppression. This value is reduced by the gas transfer suppression model to 1.06 Pg C, which is a reduction of 8 %. The W14 parameterization yields an uptake of 1.16 Pg C and with the suppression model an uptake of 1.06 Pg C which is a difference of 9 %. The decrease of the oceanic uptake using the

W14 parameterization is just calculated for comparative and example reasons to show the effect on this parameterization type. The W14 parameterization already includes an average estimate for gas transfer suppression and no suppression needs to be added on top. For the parameterization used in the Takahashi climatology (Takahashi et al., 2009), we calculated a total uptake of 1.28 Pg C without gas transfer suppression. Adding the effect of gas transfer suppression, we get a value of 1.19 Pgram C which is a reduction of 7 %. The global value from the Takahashi climatology (Takahashi et al., 2009) is 1.42 Pgram C yr^{-1}. Rödenbeck (Rödenbeck et al., 2015) estimate 1.75 Pg C yr^{-1} as uptake between 1992 and 2009. The difference between our calculation and the estimates from the global climatologies are [1] due to the different reference year, Takahashi 2000 / Rödenbeck 1992-2009 / this study 2014, which leads to different wind speed, ΔpCO_2 and SST data. [2] The data set and influence for sea ice cover is different. However, the estimated reduction of 7-9 %, due to gas transfer suppression, is also valid for the Takahashi and Rödenbeck estimates.

The DMS emissions from the ocean to the atmosphere are shown in Tab. 4. The calculated total emission from the N00 parameterization is 50.72 Tg DMS yr^{-1} for the year 2014. This is reduced, due to our gas transfer suppression calculations, to 45.47 Tg DMS yr^{-1}, which is a reduction of 11 %. The linear parameterization ZA18 estimates an emission of 56.22 Tg DMS yr^{-1}. Using the gas transfer suppression model the linear parameterization is reduced to 51.07 Tg DMS yr^{-1}, which is a reduction of 11 %. Global estimates are 54.39 Tg DMS yr^{-1} (Lana et al., 2011) and 45.5 Tg DMS yr^{-1} (Lennartz et al., 2015). Similar to the reasons we mentioned in the paragraph above, a difference in wind speed or sea ice coverage could be the reason for the difference in the global emission estimated between the Lana climatology and our calculations with the N00 parameterization. Lennartz et al. (2015) uses the water concentrations from the Lana climatology, but includes air-side DMS concentrations, which reduces the flux by 17 %. We do not include air-side DMS concentrations but gas transfer suppression, which reduces the flux by 11 %. Including both processes we can expect a reduction of 20-30 %.

The global CO_2 air-sea flux is reduced by 7-9 % due to gas transfer suppression. The impact on the DMS climatology is 11 %. This is in the range of 9.85 % which is the estimated influence of gas transfer suppression on the W14 parametrization through a different wind speed distribution. The different reduction percentages between these two gases are attributed to the larger bubble mediated gas transfer of CO_2, which compensated the loss of flux for CO_2 but not for DMS.

5 Conclusions

We provide a model to correct for the gas transfer suppression due to wind-wave interaction (Zavarsky et al., 2018). Re_{tr} and the resulting alternative wind speed u_{alt} can be calculated from standard meteorological and oceanographic variables. Additionally the condition (period, height, direction) of the ocean waves have to be known or retrieved from wave models. The calculation is iterative and can be easily implemented. The effect of the correction is shown with two data sets from the Knorr11 (Bell et al., 2017) and the SO234-2/235 cruise (Zavarsky et al., 2018). Both data sets show, after the correction, a better agreement with the linear ZA18 parameterizations (Tab. 1and Tab. 2), which only contains non suppressed gas transfer velocity measurements from the SO 234-2/235 cruise. Generally, the correction may be only applied to the interfacial gas transfer velocity k_o.

We investigated the individual measurements leading to the N00 gas transfer parameterization for the influence of gas transfer suppression. We think that the overall parameterization is heavily influenced by gas transfer suppression but, due to the measurement method (dual tracer measurements), the suppression is masked by bubble mediated gas transfer. We show a significant negative correlation between the occurrence of gas transfer suppression and the ratio of the individual measurement to the N00 parameterization. We applied a gas transfer suppression correction and fitted a new quadratic function to the corrected data set. The new parameterization is on average 22 % higher than the original N00 parameterization. This leads to the conclusion that gas transfer suppression influences gas transfer parameterizations, even if it is not directly visible, via a smaller slope.

For the W14 parameterization we used a global wind speed climatology for the year 2014 and applied the gas transfer suppression model $u_{10} \rightarrow u_{alt}$. Using the distribution function of u_{alt} we calculated a corrected gas transfer parameterization. The coefficient of the corrected parameterization is 9.85 % higher than the original one. W14 already includes the global average of gas transfer suppression. Therefore the increase, due to the correction, is expected to be less than the one for N00. The uncorrected N00 is lower than W14, but after correction N00 is larger than the corrected W14, which is expected due to the larger bubble mediated gas transfer of He and SF_6 over CO_2.

In addition, we calculated the global carbon uptake of CO_2 due to air-sea exchange and the global emission of DMS. The reduction, due to the consideration of gas transfer suppression, is between 7-9 % for CO_2 and 11 % for DMS. This is in the range of the calculated influence of gas transfer suppression on the global parameterization W14.

We think that gas transfer suppression has a global influence on air-sea gas exchange of 7-11 %. These numbers are supported by the correction of the W14 parametrization as well a global DMS and CO_2 gas transfer calculation. Local conditions may lead to much higher influences. Gas transfer velocity parameterizations from regional data sets might be heavily influenced by gas transfer suppression. We have shown this for the N00 parameterization. This should be considered with their use.

For global calculations we recommend the use of the Wanninkhof parameterizations (Wanninkhof, 2014), as it already has an average global gas transfer suppression included. We recommend using a linear parameterization (e.g. ZA18) for rather soluble gases, such as DMS, in the cases of non-suppressed gas transfer. The suppression can be determined using the Re_{tr} parameter. If conditions favor suppression, we recommend our iterative approach to correct u to u_{alt} (Fig. 1). For gases with a similar solubility as CO_2, we recommend the use of W14. In case of no gas transfer suppression, we recommend the use of the corrected W14+9.85 % parameterization. The corrected N00 (N00+22 %) parameterization is recommended for very insoluble gases with the absence of gas transfer suppression, the original N00 is recommended for the gas transfer suppressed case.

Data availability. The wave data is available at the website of the NOAA Environmental Modelling Center. The ERA-Interim data is available at the website of the ECMWF. The data is stored at the data portal of GEOMAR Kiel.

Appendix A: Directional dependencies

Figure A1 shows the shape of the wave (half sphere) as experienced by the wind flowing over it with a certain angle θ. The larger θ the more streamlined the wave (half sphere). The more streamlined the more difficult it is to generate turbulence, which counteracts the flow detachment and as a consequence gas transfer suppression.

Wind at an angle of $\theta = 90^o$ does not experience a wave crest or trough, but rather an along-wind corrugated surface. In this case there should be no gas transfer suppression. Zavarsky et al. (2018) predicts a non suppressed condition around $\mathrm{Re}_{tr} = 0$, which coincides with $\theta \approx 90^o$ or $\mathrm{u}_{tr} \rightarrow 0$. Both conditions rarely occur and must be investigated in the future.

Appendix B: Correction of wind speed or correction of k

A shift on the x-axis from u_{10} to u_{alt} is, when related to a linear relationship, equivalent to an increase of k by Δk. As gas transfer suppression only affects interfacial gas transfer we use the ZA18 parameterization, which is a linear relationship describing k_o, as a reference and correction (Eq. 12). Figure A2 illustrates the two different possibilities of correcting suppressed gas transfer values.

The correction of the two DMS data sets (SO234-2/235 and Knorr11) is done by shifting u_{10} along the x-axis to u_{alt}. We want to test whether u_{10} can be directly replaced by u_{alt} for k_o parameterizations. Gas transfer suppression corrections for bubble influenced parameterizations are done by adding Δ k, which is directly related to the difference Δu=u_{10}-u_{alt}.

Competing interests. The authors declare no competing interests.

Acknowledgements. The authors thank Kirstin Krüger, the chief scientist of the RV Sonne cruise (SO234-2/235), as well as the captain and crew. We thank the Environmental Modeling Center at the NOAA/National Weather Service for providing the WaveWatch III data. We thank the European Centre for Medium-Range Weather Forecasts for providing the ERA-Interim data. This work was carried out under the Helmholtz Young Investigator Group of C. Marandino, TRASE-EC (VH-NG-819), from the Helmholtz Association. The cruise 234-2/235 was financed by the BMBF, 03G0235A.

References

Bell, T. G., De Bruyn, W., Miller, S. D., Ward, B., Christensen, K. H., and Saltzman, E. S.: Air-sea dimethylsulfide (DMS) gas transfer in the North Atlantic: evidence for limited interfacial gas exchange at high wind speed, Atmos. Chem. Phys., 13, 11 073–11 087, https://doi.org/10.5194/acp-13-11073-2013, http://www.atmos-chem-phys.net/13/11073/2013/, 2013.

Bell, T. G., De Bruyn, W., Marandino, C. A., Miller, S. D., Law, C. S., Smith, M. J., and Saltzman, E. S.: Dimethylsulfide gas transfer coefficients from algal blooms in the Southern Ocean, Atmos. Chem. Phys., 15, 1783–1794, https://doi.org/10.5194/acp-15-1783-2015, http://www.atmos-chem-phys.net/15/1783/2015/, 2015.

Bell, T. G., Landwehr, S., Miller, S. D., de Bruyn, W. J., Callaghan, A. H., Scanlon, B., Ward, B., Yang, M., and Saltzman, E. S.: Estimation of bubble-mediated air–sea gas exchange from concurrent DMS and CO2 transfer velocities at intermediate–high wind speeds, Atmospheric Chemistry and Physics, 17, 9019–9033, https://doi.org/10.5194/acp-17-9019-2017, https://www.atmos-chem-phys.net/17/9019/2017/, 2017.

Blomquist, B. W., Brumer, S. E., Fairall, C. W., Huebert, B. J., Zappa, C. J., Brooks, I. M., Yang, M., Bariteau, L., Prytherch, J., Hare, J. E., Czerski, H., Matei, A., and Pascal, R. W.: Wind Speed and Sea State Dependencies of Air-Sea Gas Transfer: Results From the High Wind Speed Gas Exchange Study (HiWinGS), Journal of Geophysical Research: Oceans, pp. n/a–n/a, https://doi.org/10.1002/2017JC013181, http://dx.doi.org/10.1002/2017JC013181, 2017.

Dee, D. P., Uppala, S. M., Simmons, A. J., Berrisford, P., Poli, P., Kobayashi, S., Andrae, U., Balmaseda, M. A., Balsamo, G., Bauer, P., Bechtold, P., Beljaars, A. C. M., van de Berg, L., Bidlot, J., Bormann, N., Delsol, C., Dragani, R., Fuentes, M., Geer, A. J., Haimberger, L., Healy, S. B., Hersbach, H., Holm, E. V., Isaksen, L., Kållberg, P., Köhler, M., Matricardi, M., McNally, A. P., Monge-Sanz, B. M., Morcrette, J. J., Park, B. K., Peubey, C., de Rosnay, P., Tavolato, C., Thepaut, J. N., and Vitart, F.: The ERA-Interim reanalysis: configuration and performance of the data assimilation system, Quarterly Journal of the Royal Meteorological Society, 137, 553–597, https://doi.org/10.1002/qj.828, http://dx.doi.org/10.1002/qj.828, 2011.

Hanley, K. E., Belcher, S. E., and Sullivan, P. P.: A Global Climatology of Wind-Wave Interaction, Journal of Physical Oceanography, 40, 1263–1282, https://doi.org/10.1175/2010JPO4377.1, http://dx.doi.org/10.1175/2010JPO4377.1, 2010.

Komori, S., McGillis, W., and Kurose, R.: Gas Transfer at Water Surfaces, 2010, Kyoto University, http://hdl.handle.net/2433/156156, 2011.

Lana, A., Bell, T. G., Simo, R., Vallina, S. M., Ballabrera-Poy, J., Kettle, A. J., Dachs, J., Bopp, L., Saltzman, E. S., Stefels, J., Johnson, J. E., and Liss, P. S.: An updated climatology of surface dimethlysulfide concentrations and emission fluxes in the global ocean, Global Biogeochemical Cycles, 25, n/a–n/a, https://doi.org/10.1029/2010GB003850, http://dx.doi.org/10.1029/2010GB003850, 2011.

Lennartz, S. T., Krysztofiak, G., Marandino, C. A., Sinnhuber, B.-M., Tegtmeier, S., Ziska, F., Hossaini, R., Krüger, K., Montzka, S. A., Atlas, E., Oram, D. E., Keber, T., Bönisch, H., and Quack, B.: Modelling marine emissions and atmospheric distributions of halocarbons and dimethyl sulfide: the influence of prescribed water concentration vs. prescribed emissions, Atmospheric Chemistry and Physics, 15, 11 753–11 772, https://doi.org/10.5194/acp-15-11753-2015, https://www.atmos-chem-phys.net/15/11753/2015/, 2015.

Naegler, T.: Reconciliation of excess 14C-constrained global CO2 piston velocity estimates, Tellus B: Chemical and Physical Meteorology, 61, 372–384, https://doi.org/10.1111/j.1600-0889.2008.00408.x, https://doi.org/10.1111/j.1600-0889.2008.00408.x, 2009.

Nightingale, P. D., Malin, G., Law, C. S., Watson, A. J., Liss, P. S., Liddicoat, M. I., Boutin, J., and Upstill-Goddard, R. C.: In situ evaluation of air-sea gas exchange parameterizations using novel conservative and volatile tracers, Global Biogeochemical Cycles, 14, 373–387, https://doi.org/10.1029/1999GB900091, http://dx.doi.org/10.1029/1999GB900091, 2000.

Rödenbeck, C., Bakker, D. C. E., Gruber, N., Iida, Y., Jacobson, A. R., Jones, S., Landschützer, P., Metzl, N., Nakaoka, S., Olsen, A., Park, G.-H., Peylin, P., Rodgers, K. B., Sasse, T. P., Schuster, U., Shutler, J. D., Valsala, V., Wanninkhof, R., and Zeng, J.: Data-based estimates of the ocean carbon sink variability first results of the Surface Ocean pCO2 Mapping intercomparison (SOCOM), Biogeosciences, 12, 7251–7278, https://doi.org/10.5194/bg-12-7251-2015, https://www.biogeosciences.net/12/7251/2015/, 2015.

Simó, R. and Pedrós-Alió, C.: Role of vertical mixing in controlling the oceanic production of dimethyl sulphide, Nature, 402, 396–399, https://doi.org/10.1038/46516, 1999.

Takahashi, T., Sutherland, S. C., Wanninkhof, R., Sweeney, C., Feely, R. A., Chipman, D. W., Hales, B., Friederich, G., Chavez, F., Sabine, C., Watson, A., Bakker, D. C., Schuster, U., Metzl, N., Yoshikawa-Inoue, H., Ishii, M., Midorikawa, T., Nojiri, Y., Körtzinger, A., Steinhoff, T., Hoppema, M., Olafsson, J., Arnarson, T. S., Tilbrook, B., Johannessen, T., Olsen, A., Bellerby, R., Wong, C., Delille, B., Bates, N., and de Baar, H. J.: Climatological mean and decadal change in surface ocean pCO2, and net sea–air CO2 flux over the global oceans, Deep Sea Research Part II: Topical Studies in Oceanography, 56, 554 – 577, https://doi.org/http://dx.doi.org/10.1016/j.dsr2.2008.12.009, http://www.sciencedirect.com/science/article/pii/S0967064508004311, surface Ocean CO2 Variability and Vulnerabilities, 2009.

Tolman, H. L.: User manual and system documentation of WAVEWATCH-III version 1.15, NOAA / NWS / NCEP / OMB Technical Note, 151, 97, 1997.

Tolman, H. L.: User manual and system documentation of WAVEWATCH-III version 1.18, NOAA / NWS / NCEP / OMB Technical Note, 166, 110, 1999.

Tolman, H. L.: User manual and system documentation of WAVEWATCH III TM version 3.14, NOAA / NWS / NCEP / MMAB Technical Note, 276, 220, 2009.

Wanninkhof, R.: Relationship between wind speed and gas exchange over the ocean, Journal of Geophysical Research: Oceans, 97, 7373–7382, https://doi.org/10.1029/92JC00188, http://dx.doi.org/10.1029/92JC00188, 1992.

Wanninkhof, R.: Relationship between wind speed and gas exchange over the ocean revisited, Limnology and Oceanography: Methods, 12, 351–362, https://doi.org/10.4319/lom.2014.12.351, http://dx.doi.org/10.4319/lom.2014.12.351, 2014.

Wanninkhof, R., Hitchcock, G., Wiseman, W. J., Vargo, G., Ortner, P. B., Asher, W., Ho, D. T., Schlosser, P., Dickson, M.-L., Masserini, R., Fanning, K., and Zhang, J.-Z.: Gas exchange, dispersion, and biological productivity on the West Florida Shelf: Results from a Lagrangian Tracer Study, Geophysical Research Letters, 24, 1767–1770, https://doi.org/10.1029/97GL01757, http://dx.doi.org/10.1029/97GL01757, 1997.

Watson, A. J., Upstill-Goddard, R. C., and Liss, P. S.: Air-sea gas exchange in rough and stormy seas measured by a dual-tracer technique, Nature, 349, 145, http://dx.doi.org/10.1038/349145a0, 1991.

White, F.: Viscous Fluid Flow, McGraw-Hill series in mechanical engineering, McGraw-Hill, https://books.google.de/books?id=G6IeAQAAIAAJ, 1991.

Yang, M., Bell, T. G., Blomquist, B. W., Fairall, C. W., Brooks, I. M., and Nightingale, P. D.: Air-sea transfer of gas phase controlled compounds, IOP Conference Series: Earth and Environmental Science, 35, 012 011, http://stacks.iop.org/1755-1315/35/i=1/a=012011, 2016.

Zavarsky, A., Goddijn-Murphy, L., Steinhoff, T., and Marandino, C. A.: Bubble mediated gas transfer and gas transfer suppression of DMS and CO2, Journal of Geophysical Research: Atmospheres, 0, https://doi.org/10.1029/2017JD028071, https://agupubs.onlinelibrary.wiley.com/doi/abs/10.1029/2017JD028071, 2018.

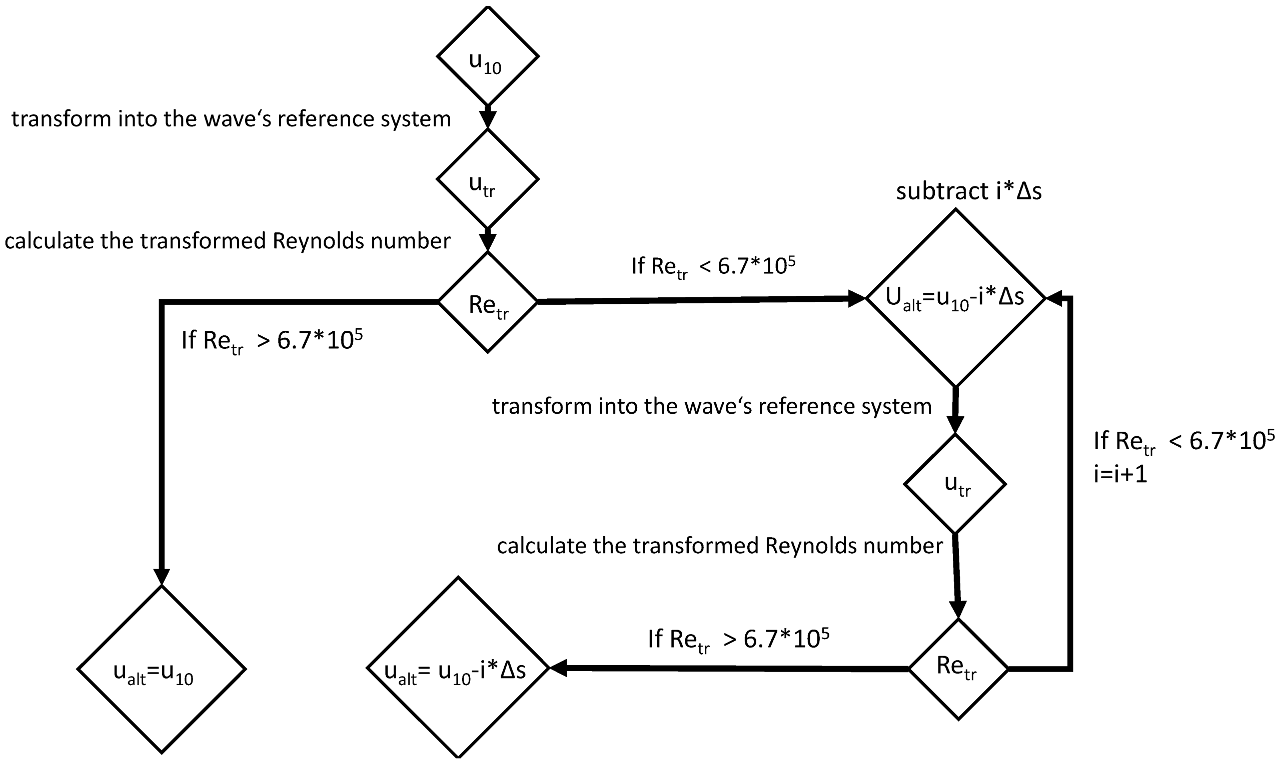

Figure 1. Work flow of the gas transfer suppression model. In the case of suppressed gas transfer, the output is the corrected wind speed u_{alt}, which then can be used in gas transfer parameterizations. The step size Δs can be adapted freely, but considerations of resolution and computing power have to be made. For this manuscript we set $\Delta s = 0.3\ m\ s^{-1}$.

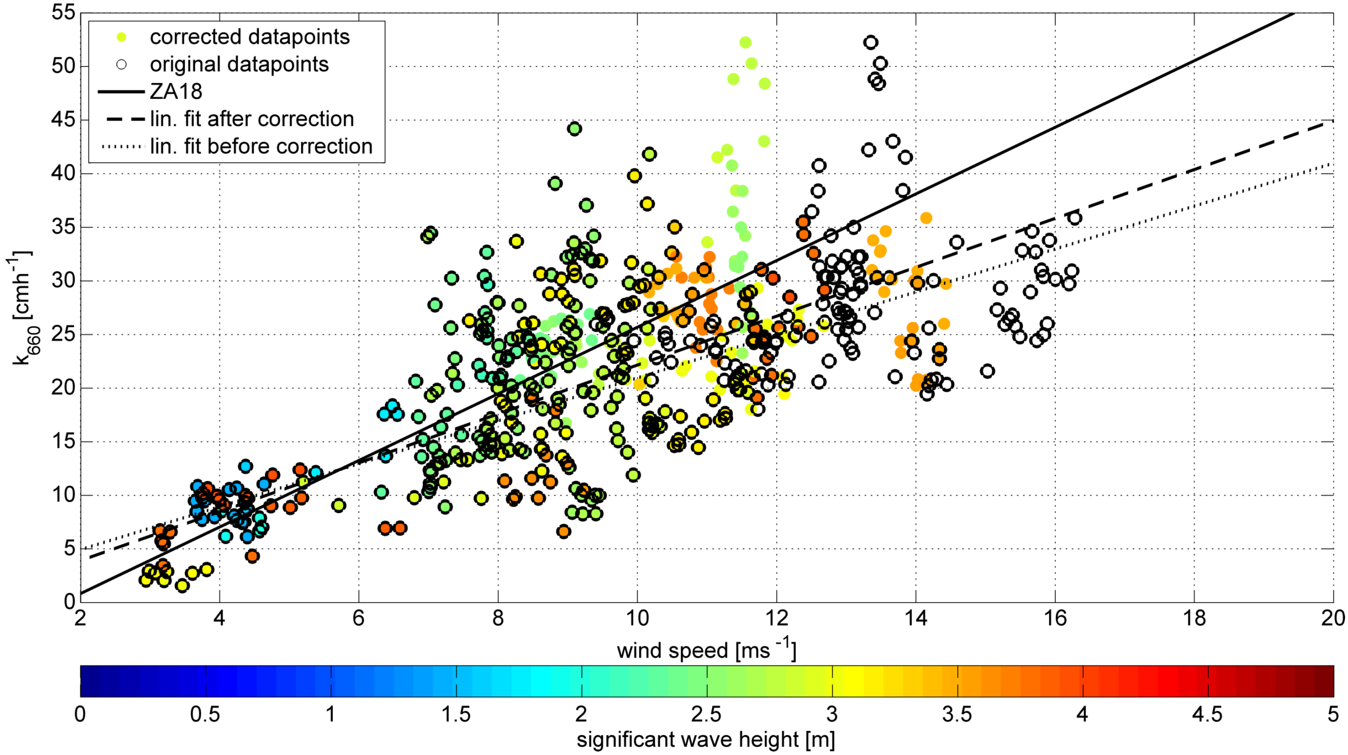

Figure 2. Correction of the SO234-2/235 DMS fluxes. The data points with $|Re_{tr}| \prec 6.96 \cdot 10^5$ were corrected using the gas transfer suppression model. Black circles denote k values at the original wind speed u_{10}. Colored filled circles denote the k value at wind speed=u_{alt}. The color shows the significant wave height. If a data point has a concentric black and filled circle, it was not corrected as it was not subject to gas transfer suppression. The black solid line is the ZA18 parameterization. The dotted line is the linear fit to the data points before the correction, the dashed line is the linear fit after the correction.

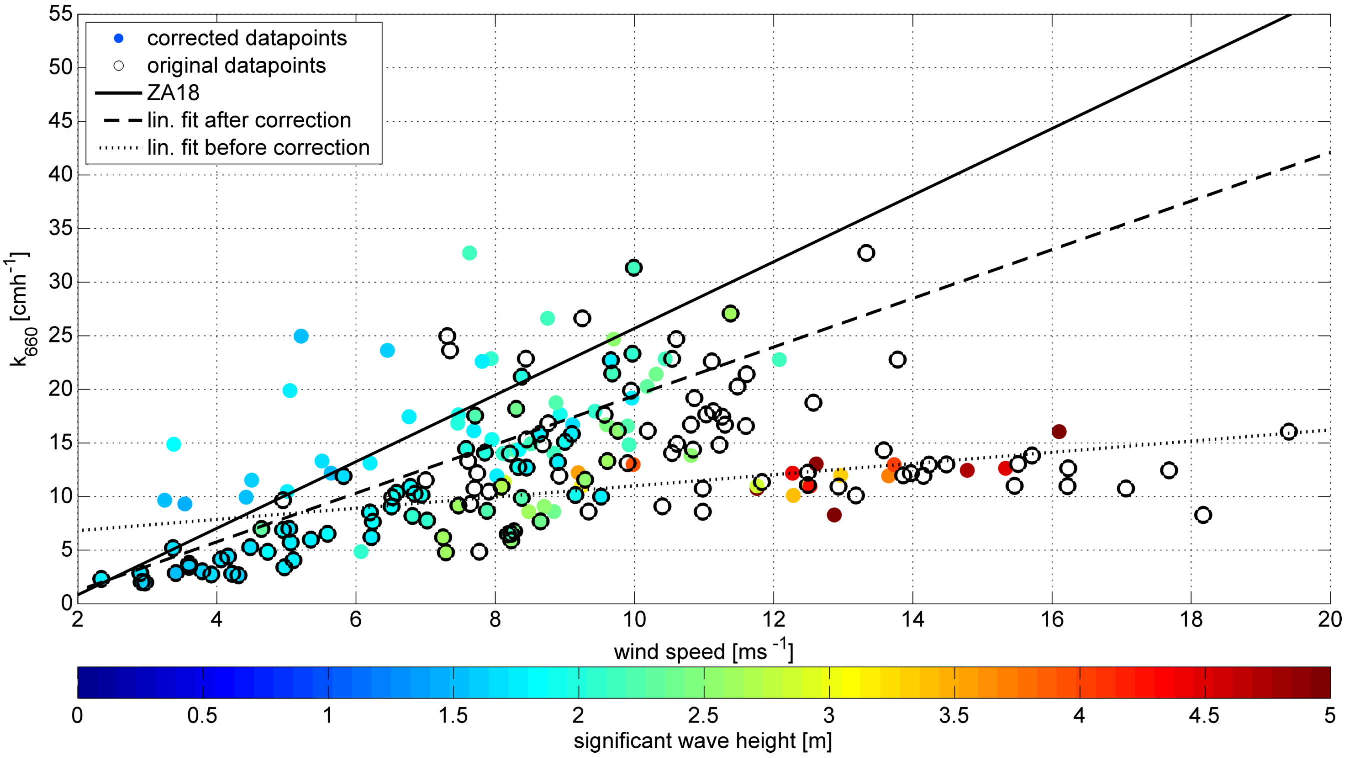

Figure 3. Correction of the Knorr11 DMS fluxes. The data points with $|Re_{tr}| \prec 6.96 \cdot 10^5$ were corrected using the gas transfer suppression model. Black circles denote k values at the original wind speed u_{10}. Colored filled circles denote the k value at wind speed=u_{alt}. The color shows the significant wave height. If a data point has a concentric black and filled circle, it was not corrected as it was not subject to gas transfer suppression. The black solid line is the ZA18 parameterization. The dotted line is the linear fit to the data points before the correction, the dashed line is the linear fit after the correction.

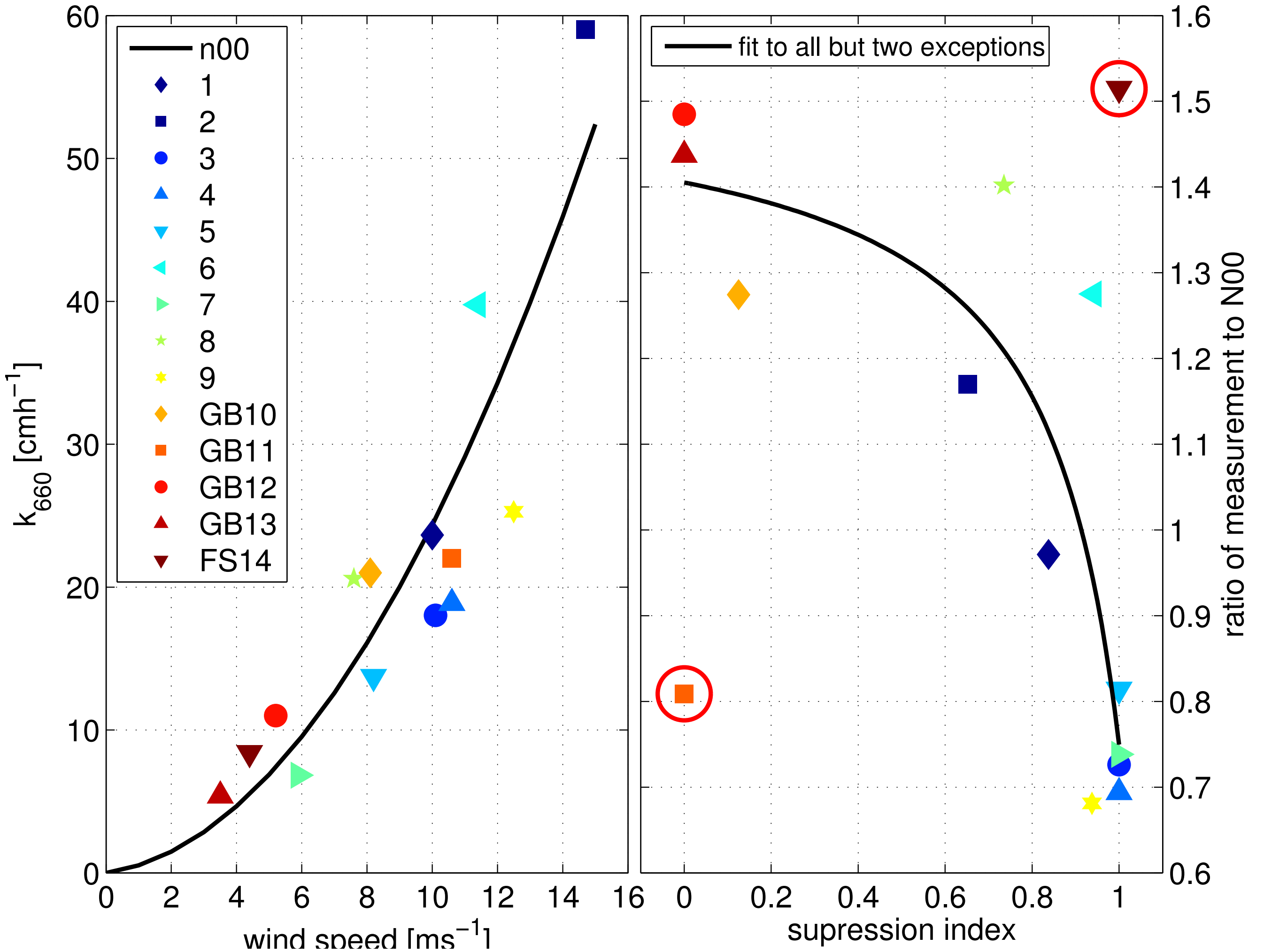

Figure 4. Individual dual tracer measurements which contribute to the N00 (solid line) parameterization [left panel]. The relationship of the gas suppression ratio to the measurement/N00 ratio [right panel]. The solid line in the right panel is a fit to the suppression to measurement/N00 relationship. A higher suppression ratio indicates a longer influence of gas transfer suppression on the data point. The two red circles denote the outlier points which are discussed in the text. The black solid line is a fit using the function $y(x) = a_1 + a_2 \cdot \frac{1}{x - a_3}$. The fit coefficients are:a_1 =1.52, a_2=0.14 and a_3=1.18 .

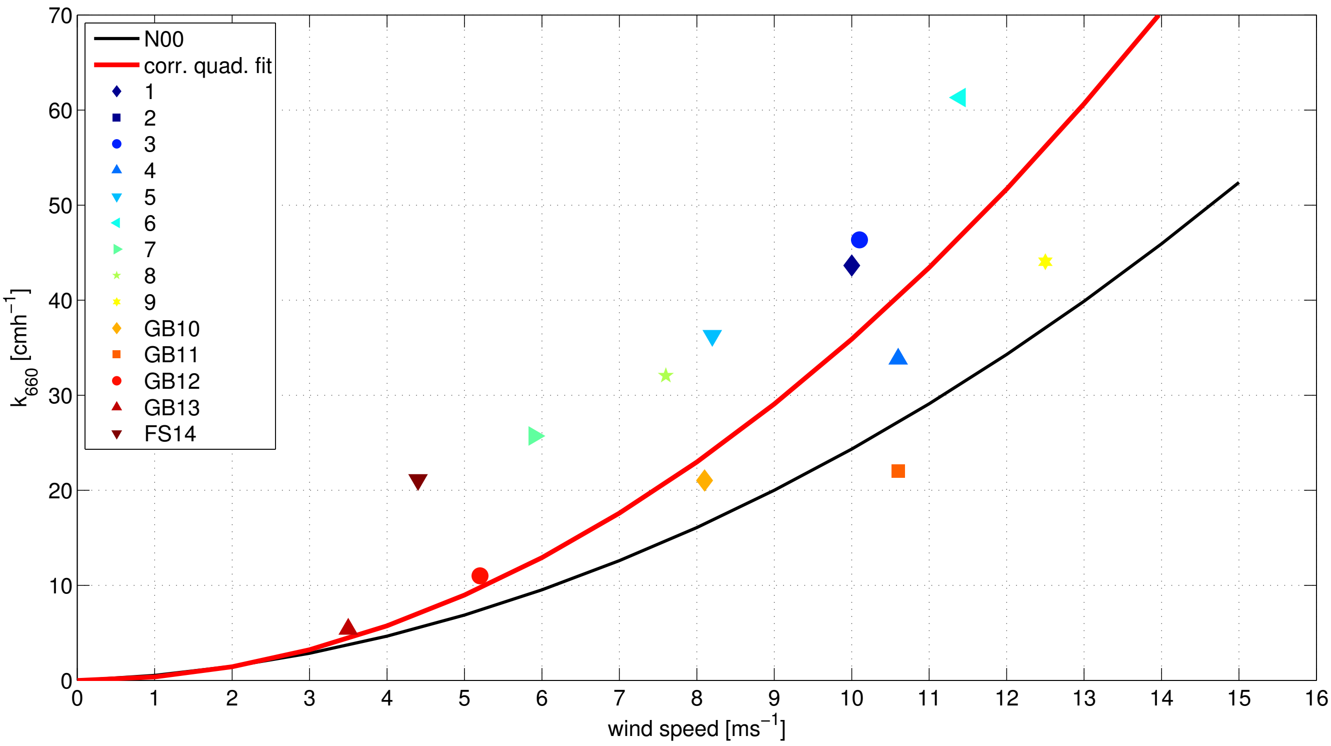

Figure 5. Corrected individual measurements, comprising the N00 parameterization, resulting from the algorithm described in Sect. 3. The difference between u_{alt} and the original u_{10} was added to k using the linear parameterization ZA18, which corrects the suppression of ko due to wind-wave interaction. This is correcting the suppression of k_o due to wind-wave interaction. The black solid line is the original N00 parametrization. The red line is a new quadratic fit to the corrected data points $k=0.359*u^2$.

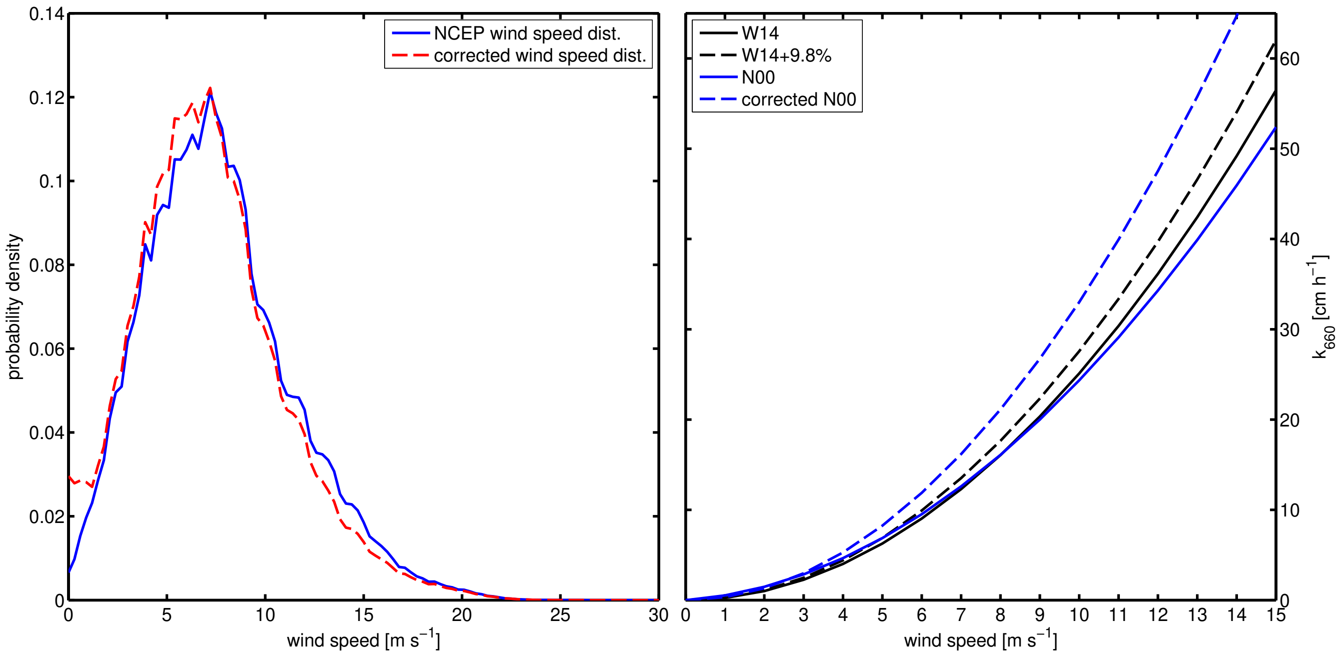

Figure 6. Wind speed distributions for the year 2014 [left panel]. The solid line is NCEP derived wind speed distribution, the dashed line the wind speed distribution of the corrected wind speed u_{alt}. Comparison of original and suppression corrected k vs wind speed parameterizations [right panel].

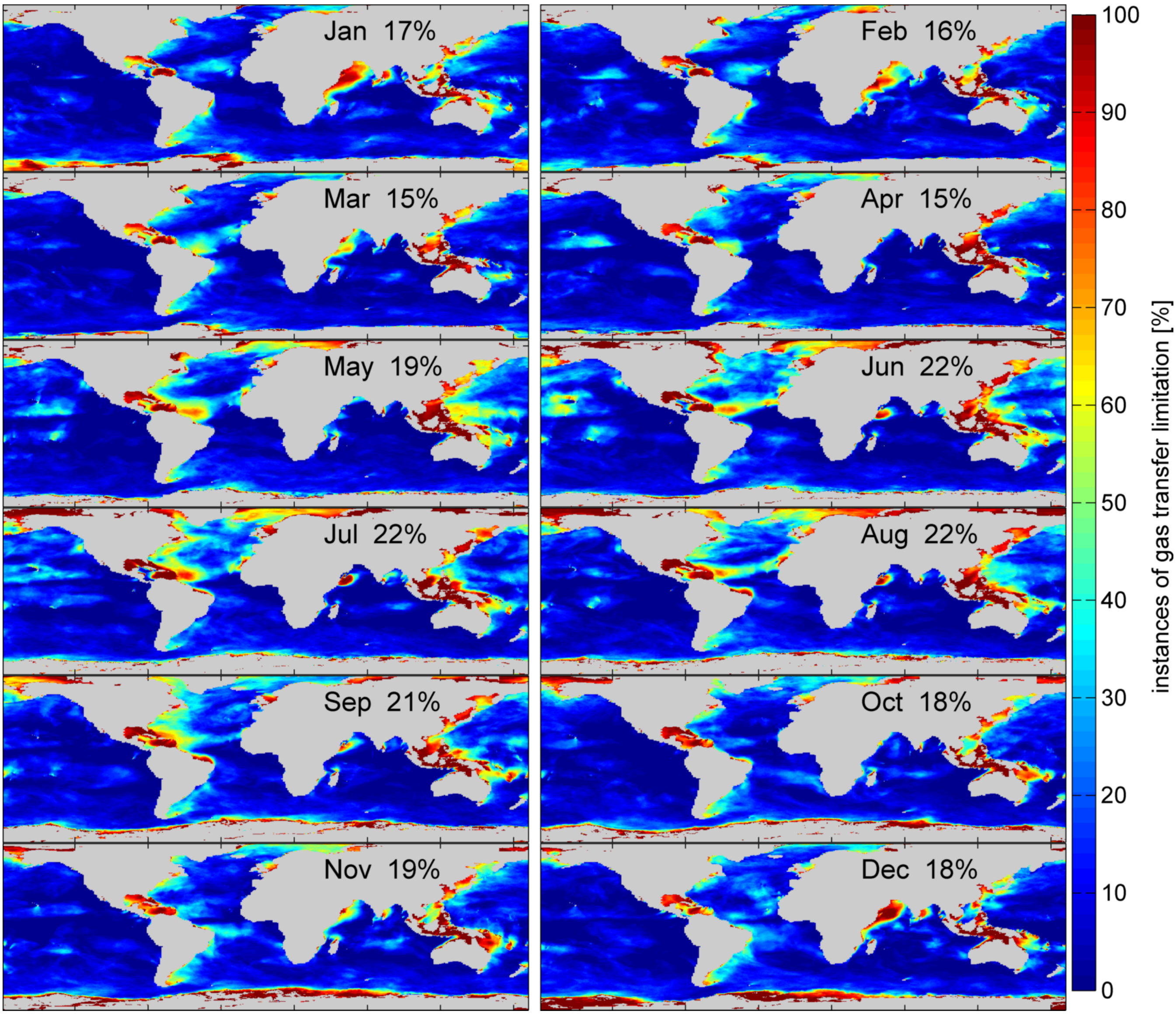

Figure 7. The global probability of experiencing gas transfer suppression during the respective month (2014). The percentage is the number of gas transfer suppressed occurrences with respect to the total data points with a 3 h resolution.

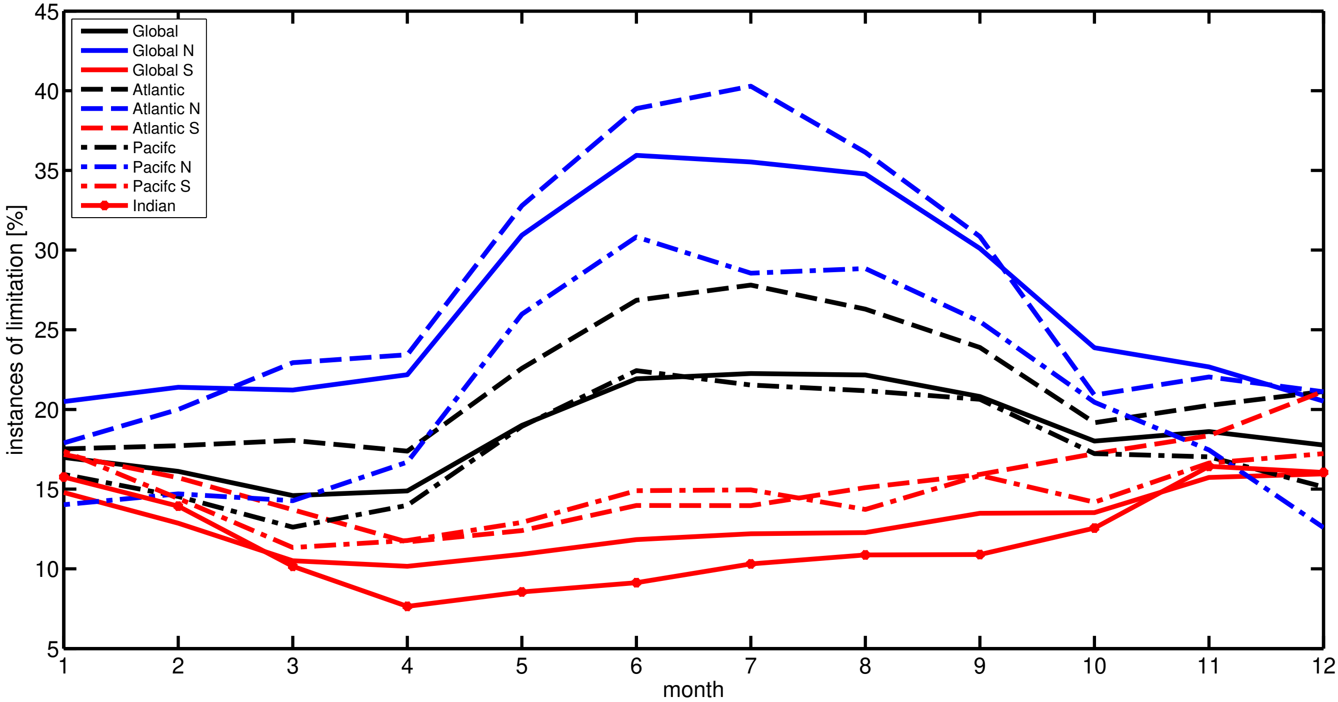

Figure 8. The probability of experiencing gas transfer suppression during the respective month (2014) divided into ocean basins and hemisphere. The Southern Ocean was added to the southern part of the respective ocean basin. The percentage is the number of gas transfer suppressed instances with respect to the total data points with a 3 h resolution.

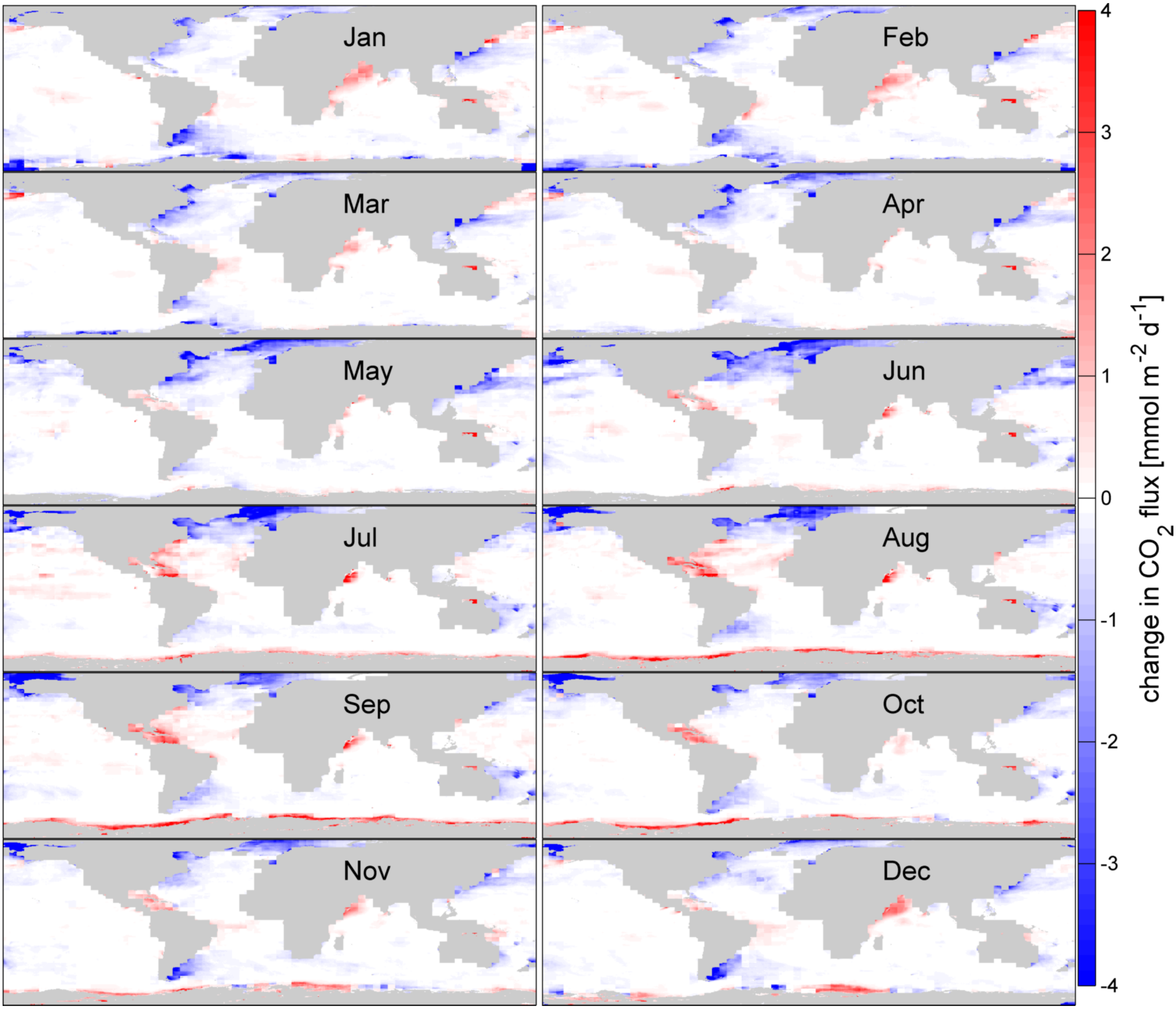

Figure 9. The absolute change of CO_2 gas transfer due to suppression for each month of 2014. Negative values (blue) denote areas where a flux into the ocean is reduced by the shown value. Positive values denote areas where flux out of the ocean is reduced by the shown value. The change is calculated using the bulk flux formula (Eq. 1) and Δk (Eq. 12).

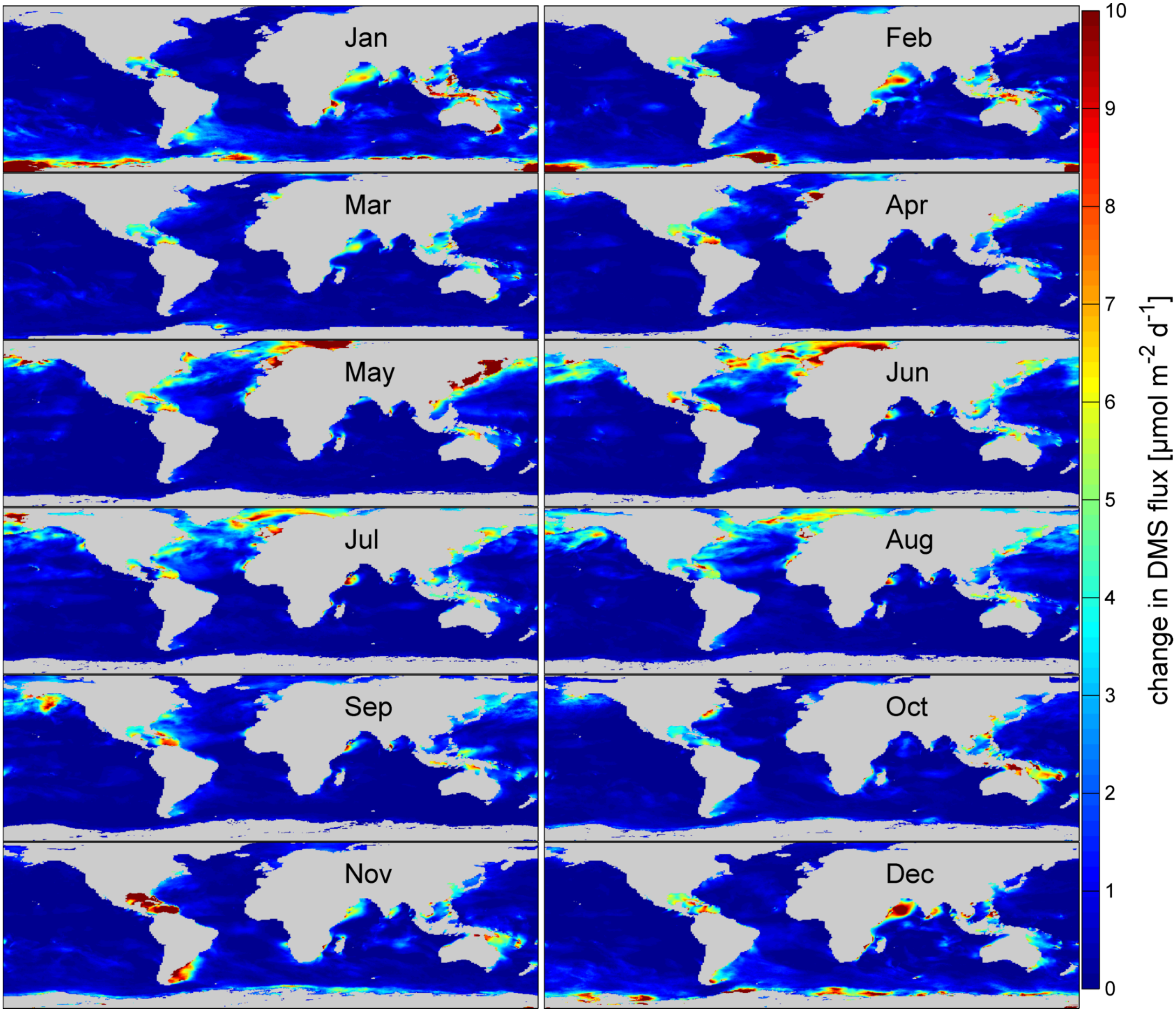

Figure 10. The absolute change of DMS gas transfer due to suppression for each month of 2014. The shown magnitudes denote the reduction by gas transfer suppression. The change is calculated using the bulk flux formula (Eq. 1) and Δk (Eq. 12).

reference fit all [cm h^{-1}]	SO234-2/235 mean diff.	Knorr11 mean diff.	SO234-2/235 mean(||)	Knorr11 mean(||)
lin. fit SO234-2/235 to corrected	-1.2	-6.96	5.5	8.1
lin. fit SO234-2/235 to uncorrected	-2.8	-10.3	6.4	10.7

Table 1. Mean differences between the fits in column one and the corrected and the uncorrected k data sets. A negative value describes that the fit, on average, overestimates the actual measured data. The mean of the absolute value is presented in the last two columns.

	Knorr11	SO234-2/235
uncorrected	$k_{660} = 0.52 \pm 0.4 \cdot u + 5.79 \pm 4.82$	$k_{660} = 2 \pm 0.42 \cdot u + 0.94 \pm 2.48$
corrected	$k_{660} = 2.27 \pm 0.5 \cdot u - 3.29 \pm 4.08$	$k_{660} = 2.28 \pm 0.45 \cdot u - 0.63 \pm 4.14$

Table 2. Linear fits to the corrected and uncorrected data sets of Knorr11 and SO234-2/235. The error estimates correspond to a 95 % confidence interval.

parameterization	flux [Pg C]
N00	1.15
N00 Re_{tr}	1.06
W14	1.16
W14 Re_{tr}	1.06
Tak09	1.28
Tak09 Re_{tr}	1.19
Takahashi 2009 (Takahashi et al., 2009)	1.42 Pg yr^{-1}
Rödenbeck (Rödenbeck et al., 2015)	1.75 Pg yr^{-1}

Table 3. 2014 carbon flux in Pg. Re_{tr} indicates an application of the gas transfer suppression model. The last two lines are estimates from previously published work.

parameterization	flux [Tg DMS yr^{-1}]
N00	50.72
N00 Re_{tr}	45.47
ZA18	56.22
ZA18 Re_{tr}	51.07
Lana et al. (2011)	54.39 Tg DMS yr^{-1}
Lennartz et al. (2015)	45.5 Tg DMS yr^{-1}

Table 4. 2014 DMS flux in Tg. Re_{tr} indicates an application of the gas transfer suppression model. The last two lines are estimated from global climatologies

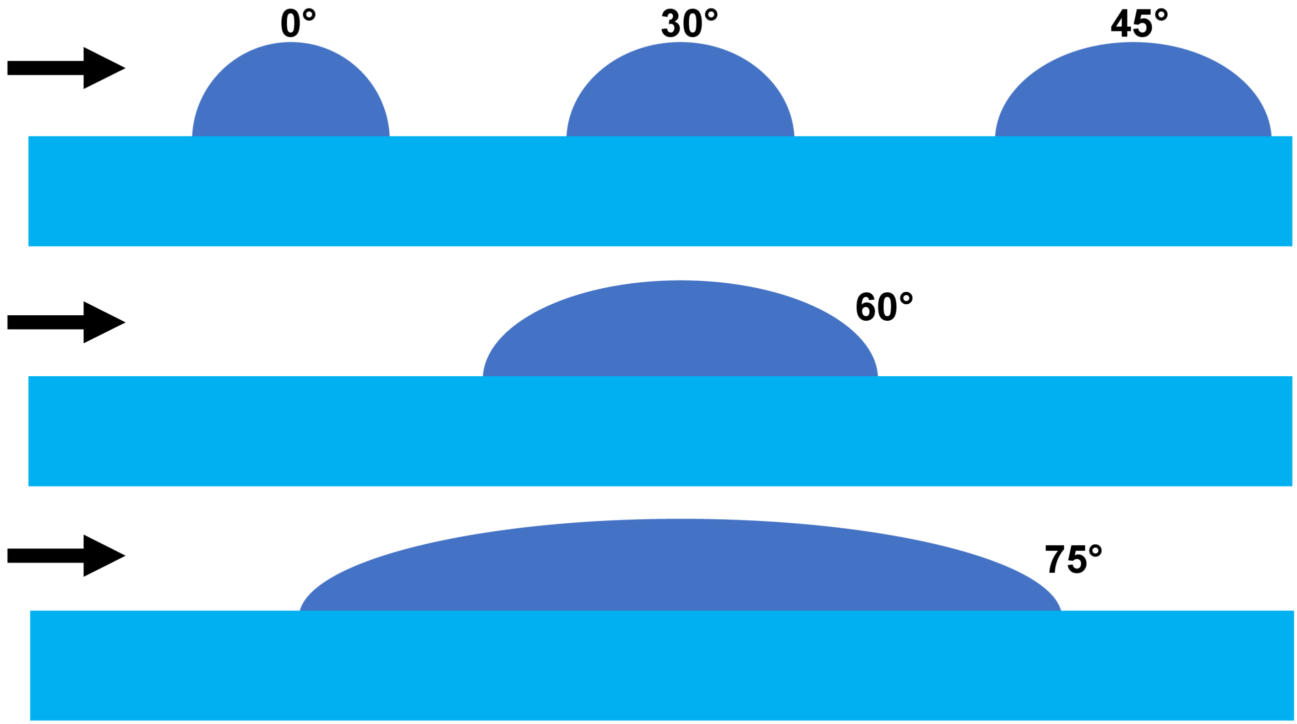

Figure A1. The streamlined shape of a wave (cylindrical half sphere) that experiences wind flowing over it from various angles, θ.

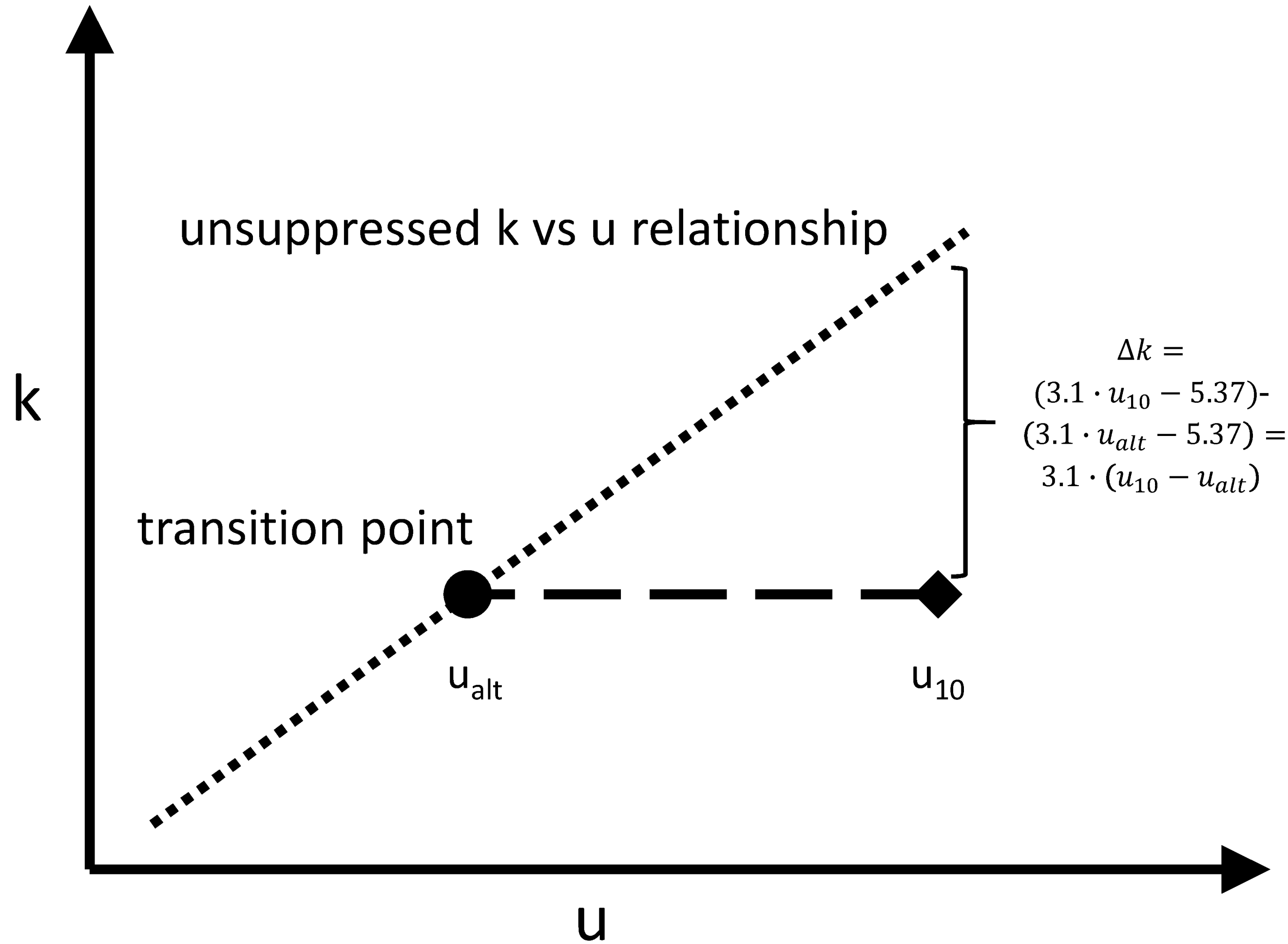

Figure A2. Illustration of the gas transfer suppression correction along either the wind speed or gas transfer velocity axis.